A Comparison of Precipitation Occurrence from the NCEP Stage IV QPE Product and the *CloudSat* Cloud Profiling Radar

MARK SMALLEY AND TRISTAN L'ECUYER

University of Wisconsin—Madison, Madison, Wisconsin

MATTHEW LEBSOCK

Jet Propulsion Laboratory, California Institute of Technology, Pasadena, California

JOHN HAYNES

Cooperative Institute for Research in the Atmosphere, Colorado State University, Fort Collins, Colorado

(Manuscript received 20 March 2013, in final form 27 August 2013)

ABSTRACT

Because of its extensive quality control procedures and uniform space–time grid, the NCEP Stage IV merged Weather Surveillance Radar-1988 Doppler (WSR-88D) radar and surface rain gauge dataset is often considered to be the best long-term gridded dataset of precipitation observations covering the contiguous United States. Stage IV accumulations are employed in a variety of applications, and while the WSR-88D systems are well suited for observing heavy rain events that are likely to affect flooding, limitations in surface radar and gauge measurements can result in missed precipitation, especially near topography and in the western United States. This paper compares hourly Stage IV observations of precipitation occurrence to collocated observations from the 94-GHz *CloudSat* Cloud Profiling Radar, which provides excellent sensitivity to light and frozen precipitation. Statistics from 4 yr of comparisons show that the *CloudSat* observes precipitation considerably more frequently than the Stage IV dataset, especially in northern states where frozen precipitation is prevalent in the cold season. The skill of Stage IV for precipitation detection is found to decline rapidly when the near-surface air temperature falls below 0°C. As a result, agreement between Stage IV and *CloudSat* tends to be best in the southeast, where radar coverage is good and moderate-to-heavy liquid precipitation dominates. Stage IV and *CloudSat* precipitation detection characteristics are documented for each of the individual river forecast centers that contribute to the Stage IV dataset to provide guidance regarding potential sampling biases that may impact hydrologic applications.

1. Introduction

The inherent variability in precipitation over the contiguous United States (CONUS) is responsible for flooding and droughts, drives fluctuations in freshwater supplies, and has significant implications for the nation's agricultural output. The benefits of accurate precipitation monitoring and prediction are clear, and long-term, high-resolution precipitation datasets are critical to the hydrology and climate communities.

The National Centers for Environmental Prediction (NCEP) Stage IV consists of hourly precipitation accumulations on a ~4.7-km polar stereographic grid across the CONUS beginning in 2001 (Lin and Mitchell 2005). The production process utilizes a combination of the national Weather Surveillance Radar-1988 Doppler (WSR-88D) network of ground radars and surface gauges. The NCEP Stage IV accumulations are computed as a national mosaic of the multisensor precipitation estimator (MPE), which is a fusion of the digital precipitation arrays (DPAs) from the National Weather Service (NWS) Precipitation Processing System (PPS; originally at polar 1° × 1 km resolution) with available surface gauges at each of the 12 CONUS River Forecast Centers (RFCs; Fulton et al. 1998; Lin and Mitchell 2005). The

Corresponding author address: Mark Smalley, Dept. of Atmospheric and Oceanic Sciences, University of Wisconsin—Madison, 1225 W. Dayton St., Madison, WI 53706.
E-mail: smalley2@wisc.edu

DOI: 10.1175/JHM-D-13-048.1

MPE (and therefore the Stage IV) benefits both from surface gauge input and manual and automatic quality controls at each individual RFC before being interpolated to the Hydrologic Rainfall Analysis Project (HRAP) grid to become the NCEP Stage IV (Fulton 2005). This product is widely considered to be the best gridded rain accumulation dataset over the CONUS and is frequently employed as the benchmark, or truth, when evaluating other remotely sensed precipitation products (Wu et al. 2012; Gourley et al. 2010; Tesfagiorgis et al. 2011; Lin and Hou 2012). The Stage IV has many applications, including forecast verification (e.g., Yuan et al. 2005, 2007), validation of downscaling models (Tao and Barros 2010), and has been used as an input to the Eta–Eta Data Assimilation System (EDAS; Lin and Mitchell 2005) precipitation assimilation routine, to name a few.

Several studies have attempted to assess the performance the Stage IV accumulations with surface rain gauge networks and other ground radar products. For example, Habib et al. (2009) found that comparisons with independent surface gauges are good when measured over long time periods, but they also identified large differences for individual rain events. Habib et al. (2013) found that, when comparing different realizations of the MPE (e.g., with and without gauges and mean-field and local bias corrections from surface gauges), the best match to measurements from an independent surface gauge network was the product that was quality controlled by RFC forecasters and chosen to represent the best estimate of the rain field in hydrologic applications like Stage IV. The quality controlled quantitative precipitation estimation (QPE) showed a high probability of detection, a low probability of false detection, and relatively low standard deviations of random error at all rainfall thresholds used in the study, reflecting the value of human input to the Stage IV. These two studies were performed near the Gulf of Mexico in Louisiana, so effects of frozen precipitation were not considered. Westcott et al. (2008) found that daily and monthly Stage IV accumulations were generally within 25% of those from independent surface gauges. However, the general scarcity of surface gauges caused these and other preceding Stage IV comparisons to include only a few validation points in each Stage IV grid box that cannot represent the subgrid variability that often characterizes precipitation across the United States.

Comparisons with other radar products (Westcott et al. 2008; Gourley et al. 2010) have shown that Stage IV outperforms radar-only products and radar-gauge products with no manual quality control. These studies, however, cannot assess issues of beam blockage and beam overshoot since all datasets use the same radars and therefore give the reader an optimistic view of the performance of Stage IV. These issues, which are illustrated in Maddox et al. (2002, their Fig. 5a) and in Cao et al. (2013), result in large gaps in coverage below 2 km above ground level, especially in the mountains and western regions, where precipitation is often forced by orographic lifting. WSR-88D radars may also underestimate some lake effect precipitation events because of beam overshoot (Nicosia et al. 1999). The effective ranges of WSR-88D radars are also affected by the height of the freezing level, which determines the location of the brightband and changes with region, season, and synoptic conditions. Stage IV grid points that fall outside the effective range of all radars due to any of these effects are either interpolated from nearby MPE points or are filled with Geostationary Operational Environmental Satellite (GOES) infrared brightness temperature rain rate estimates as part of the manual quality control at individual RFCs (Fulton 2005). While this interpolation undoubtedly helps to fill gaps in radar-only datasets, the quality of the rainfall estimates in interpolated regions is difficult to assess using conventional ground-based instrumentation.

Frozen precipitation also poses difficulties to radar- and gauge-derived liquid-equivalent precipitation rates. The NWS PPS assumes the existence of spherical hydrometeors and does not distinguish between liquid and frozen hydrometeor types (Fulton et al. 1998). This assumption in the dynamic Z–R relationships causes biases when dealing with frozen precipitation or when the radar beam crosses above the freezing layer in any season (Zhang et al. 2008; Zhang and Qi 2010). Additionally, the effective range of the WSR-88D radar is reduced when winter conditions lower the freezing level or create temperature inversions (Fulton 2005). This causes an increased dependence on surface gauges, which have their own difficulties with blowing snow and spatial coverage. Many of these difficulties are reviewed by Michaelides et al. (2009). These effects are more likely to impact the western CONUS, as the WSR-88D network is much denser in the eastern CONUS.

In summary, many studies have shown that Stage IV outperforms other radar-only, gauge-only, and satellite retrievals, but the absolute performance of the Stage IV dataset for characterizing the frequency of occurrence of precipitation remains an open question. While many applications using Stage IV data often focus on moderate-to-heavy rainfall events, there are several hydrologic, agricultural, air quality, and transportation applications that also require precipitation occurrence to be accurately prescribed. This study compares precipitation frequency from the multisensor Stage IV across the CONUS to those from the polar orbiting *CloudSat* Cloud Profiling Radar (CPR; Stephens et al. 2008). The objective is to

characterize the strengths and weaknesses of each of these ground-based and satellite platforms for detecting precipitation and to attribute discrepancies to the characteristics of each observing system in different environments. While each dataset is found to miss some precipitation, the results suggest that the −30 dBZ sensitivity of the W-band CPR (Tanelli et al. 2008), the strong attenuation signature of precipitation at this wavelength, and the relatively uniform 750-m height of reflectivities used in the *CloudSat* precipitation detection algorithm (Haynes et al. 2009) make it an excellent reference for identifying rainfall and snowfall.

2. Data

a. *Stage IV*

Hourly NCEP Stage IV (Lin and Mitchell 2005) precipitation accumulations from the years 2007 to 2010 were obtained from the Stage IV QPE distribution website (http://www.emc.ncep.noaa.gov/mmb/ylin/pcpanl/stage4/). As noted earlier, the Stage IV QPE product utilizes manual and automatic quality controls within each of the individual RFCs and benefits from a high-resolution 4.7-km grid, but it is still susceptible to unavoidable uncertainties from beam blockage, beam overshoot, reduced sensitivity at long ranges, and scarcity of surface gauges. For the purposes of this study, the Stage IV data are converted to a binary discrimination of precipitation or no-precipitation based on the presence of nonzero rain accumulations in each Stage IV grid box in the given hour. All reported Stage IV accumulations greater than zero are set to one, designating a precipitating retrieval. Precipitation estimates over the oceans, Canada, and Mexico are omitted from this study, as the goal is to examine the precipitation detection characteristics of Stage IV over regions relevant for hydrologic applications over the CONUS. Figure 1 shows the definitions of the RFC basins and the coverage of the precipitation accumulations examined here. Note that the state of Washington and surrounding area is not represented in the 1-h Stage IV data product.

b. CloudSat *rainfall detection product*

The 94-GHz CPR flies aboard the polar-orbiting *CloudSat* satellite in NASA's A-Train constellation. *CloudSat* observes a single along-track nadir reflectivity curtain with a spatial resolution of about 1.4 km × 1.8 km and a minimum detection signal of −30 dBZ. *CloudSat* launched in 2006 and provides a multiyear record with 5–6 overpasses of the CONUS each day at close to 0130 and 1330 local time (LT). Its observations have recently been used to provide new global rainfall

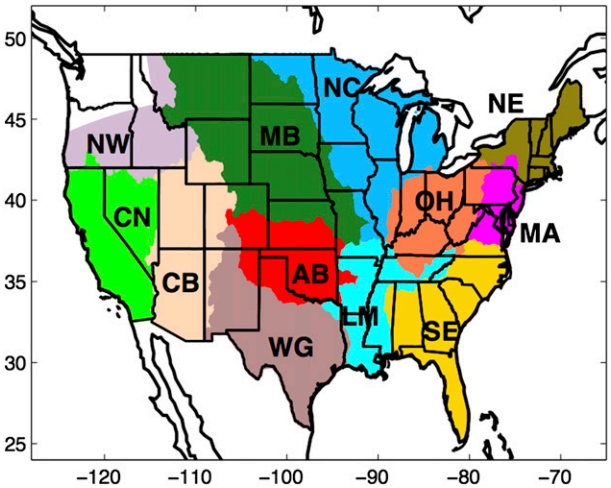

FIG. 1. Stage IV precipitation accumulation coverage for the Northwest (NW), California–Nevada (CN), Colorado Basin (CB), Missouri Basin (MB), Arkansas–Red Basin (AB), West Gulf (WG), North Central (NC), Lower Mississippi (LM), Ohio (OH), Northeast (NE), Middle Atlantic (MA), and Southeast (SE) RFC basins. Study coverage is limited to the CONUS.

and snowfall datasets (L'Ecuyer and Stephens 2002; Haynes et al. 2009; Lebsock and L'Ecuyer 2011). Comparisons against satellite-based passive microwave and Ku-band radar precipitation observations emphasize the enhanced sensitivity of *CloudSat* to light precipitation (Berg et al. 2010; Behrangi et al. 2012).

This study focuses on the *CloudSat* precipitation occurrence dataset, 2C-PRECIP-COLUMN (release 04) initially described in Haynes et al. (2009). The original algorithm applies thresholds to attenuation and multiple-scattering-corrected, near-surface reflectivities and an estimate of path-integrated attenuation derived from the surface backscatter cross section to assess the likelihood of precipitation falling in the atmospheric layer between 750 and 1000 m over open ocean surfaces. Preliminary comparisons of rainfall frequency in the 2C-PRECIP-COLUMN dataset against selected rain gauges from diverse locations around the globe are encouraging (Ellis et al. 2009). However, the original dataset did not consider land or sea ice surfaces. The open ocean algorithm uses the path-integrated attenuation (PIA) as an input. It must be modified over land surfaces because there are currently no reliable estimates of PIA over these surfaces.

The method to extend the determination of surface precipitation occurrence over land and ice surfaces to the 2C-PRECIP-COLUMN product is described here. This method follows a relatively simple decision tree that employs temperature-dependent reflectivity thresholds. To begin, a phase determination of rain, mixed, or snow is

made using the maximum tropospheric temperature (T_{max}) in the *CloudSat* observation profile provided in the European Center for Medium-Range Weather Forecasts (ECMWF) analysis. If $T_{max} > 275$ K then the phase is set to rain, if $T_{max} < 273$ K then the phase is set to snow, and between these thresholds the phase is determined as mixed. The mixed phase determination should be interpreted conservatively as an uncertain categorization. Following phase determination, the precipitation occurrence is determined using the reflectivity profile of the lowest discernible cloud layer, which is defined as the lowest layer where the value of the *CloudSat* geometric profile product (2B-GEOPROF) cloud mask (Marchand et al. 2008) is greater than 30. A complication of precipitation determination from the 94-GHz spaceborne radar is the attenuation of the radar beam, which can substantially diminish the reflectivity signal near the surface, therefore requiring a methodology slightly more sophisticated than using a threshold on the near-surface reflectivity. The occurrence algorithm is distilled to four variables: the reflectivity in the fifth radar bin above the surface (~1200 m; Z_5), the cloud layer maximum reflectivity (Z_{max}), the cloud layer cloud base height (H_{base}), and the surface radar cross section (σ_0). In the case of rain, a classification of "certain" requires either that $Z_5 > 5$ dBZ or that there is evidence of heavy attenuation in the variables Z_{max}, H_{base}, and σ_0. For mixed phase, the certain classification reflectivity threshold is $Z_5 > -2.5$ dBZ, with an additional check for attenuation given that significant amounts of liquid water are most certainly present for these scenarios. For snow, the certain classification is determined using the threshold $Z_5 > -5$ dBZ with no additional checks on attenuation because the attenuation by ice at 94 GHZ is generally small and tends to be compensated by multiple-scattering effects (Matrosov and Battaglia 2009). The reflectivity thresholds applied here to land and ice surfaces represent adjustments to the quantitative thresholds provided in Haynes et al. (2009), corresponding to precipitation rates of 0.03 mm h^{-1}. Upward threshold adjustments are necessary over solid surfaces because the precipitation detection algorithm is applied in the fifth above-surface bin (~1200 m) instead of the third bin (~750 m) above the surface in order to avoid contamination of the atmospheric signal with the surface return. The adjusted precipitation thresholds were determined through a combination of quantitative comparisons of 1 yr of coincident overpasses of *CloudSat* and the C-band weather radar located at King City, Ontario, Canada, which are described in Hudak et al. (2008), and qualitative visual inspection of *CloudSat* observations.

In the analysis that follows, the Precip_flag precipitation diagnostic from 2C-PRECIP-COLUMN is considered in the context of rainfall occurrence estimates from the Stage IV dataset. Only fields of view (FOVs) labeled as rain certain, snow certain, or mixed certain are considered in this study.

c. Spatial scaling

The fractional occurrence of precipitation is a strong function of the spatial scale over which precipitation is identified (Berg et al. 2010; Stephens et al. 2010). To account for the different spatial resolutions of Stage IV and *CloudSat*, binary precipitation detection retrievals from *CloudSat* are smoothed over 5 FOVs and any resulting FOVs with smoothed values greater than 0 are set to 1 to approximate the resolution of the Stage IV QPEs. With a *CloudSat* nominal FOV separation of ~1.1 km, this reduces the *CloudSat* resolution to ~5 km, which is much closer to the nominal Stage IV resolution of ~4.7 km. The resulting scaled *CloudSat* retrievals therefore represent the maximum precipitation fraction over each overlapping 5-km along-track segment as opposed to detecting precipitation based on mean reflectivities over the segment. However, this more closely resembles Stage IV rainfall occurrence that effectively combines rainfall information contained in constituent azimuthal 1° km × 1 km polar grid boxes into the final 4.7-km gridded product (Fulton et al. 1998). The effects of scaling the *CloudSat* data are investigated in the appendix, where it is shown that while the scaling does increase the number of detections made by *CloudSat*, it does not significantly affect the conclusions of the study.

d. Collocation

Stage IV retrievals are collocated with overpassing *CloudSat* retrievals by a nearest-neighbor method. There are a total of 8196 overpasses during the years 2007–10, yielding 2 988 257 collocated observations where both *CloudSat* and Stage IV produce a valid retrieval. In the record, 154 198 (5.2%) collocated Stage IV FOVs contain precipitation and 271 759 (9.1%) scaled and collocated *CloudSat* FOVs contain precipitation. Although the collocation process requires that the centers of any two collocated FOVs be within 3 km of each other, there are unavoidable uncertainties stemming from the fact that the Stage IV measures precipitation rates for the duration of 1 h, while the *CloudSat* scan of each FOV is very brief, about 0.16 s. It is expected that collocation alone will cause precipitation to be measured by one dataset but not the other. For example, in a given collocated pair, it is possible for a cloud to stop precipitating before the *CloudSat* overpass or for the *CloudSat* overpass to occur before the onset of precipitation during that Stage IV measurement hour. This can happen anywhere, but it may be more

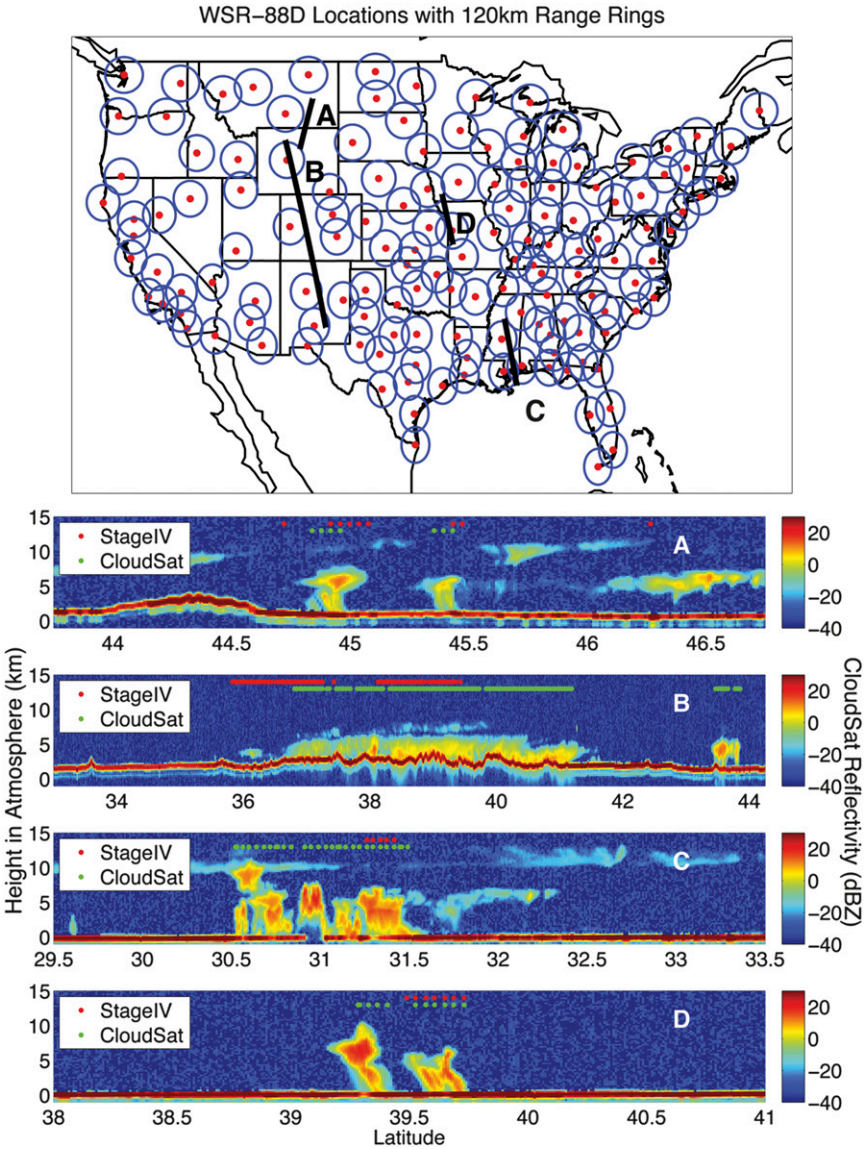

FIG. 2. Map of WSR-88D locations (red dots) with 120-km range rings (blue circles). Black lines indicate respective locations of selected *CloudSat* reflectivity curtains depicted below the map where locations of *CloudSat* and Stage IV precipitation detections are shown as green and red dots, respectively. The reflectivity curtains shown as orbits (top to bottom) A, B, C, and D were taken from the 1 Jul 2008 orbit 11577, 1 Feb 2008 orbit 09385, 11 Oct 2009 orbit 18384, and 2 Jul 2008 orbit 11598 *CloudSat* 2B-GEOPROF files, respectively.

prevalent in areas of spotty convection or fast-moving systems. The reverse is not possible because *CloudSat* measurements are effectively instantaneous in comparison to Stage IV 1-h accumulation periods. Therefore, this effect will serve to increase the Stage IV detection rate in comparison to *CloudSat*.

Figure 2 presents four example overpasses with locations of collocated Stage IV and *CloudSat* precipitation flags with *CloudSat* reflectivities shown as a reference. These examples show how detection differences can arise from both physical and collocation-based means. For reference, corresponding *CloudSat* footprints are outlined in black on the map, showing WSR-88D locations with 120-km range rings. While 120 km is well within the 230-km range of the WSR-88D radars, it was chosen to resemble the spacing of Fig. 5a in Maddox et al. (2002), which shows ranges at 2 km above ground level. From overpass A in Fig. 2, it can be inferred that the precipitating environment changed at some point during the Stage IV hour of accumulation, and the brief

CloudSat overpass witnessed only a snapshot of the precipitation pattern. The rain system may have had an east–west propagation that brought the 44.7° and 46.3° precipitation events out of the path of *CloudSat*, or precipitation could have ended before or started after the *CloudSat* overpass. Another possible explanation of the offset is a heavier reliance on gauge interpolation in this area because of the long distance to the nearest radar. Stage IV and *CloudSat* could also be making their retrievals at different heights in the atmosphere, which could make comparisons sensitive to high winds and potentially to evaporation. Offsets like these are not necessarily errors in either precipitation retrieval, but they contribute unavoidably to differences in statistics between the two datasets. Orbit section B in Fig. 2 shows how the Stage IV may miss precipitation over mountains, where beam blockage and spatial coverage often limit ground radar detection capabilities. Overpass C in Fig. 2 shows a case where precipitation is strong enough to totally attenuate the *CloudSat* radar at 31°, but Stage IV does not report precipitation in an area of seemingly good radar coverage. The fourth example D shows snow falling over western Missouri in a high-shear environment. Detection differences may also arise when Stage IV accumulations result from WSR-88D systems sensing the upper portion of precipitation, but then high winds blow snow into a nearby Stage IV grid box, at which time *CloudSat* samples a lower portion of the precipitating atmosphere and therefore senses the precipitation at a different location. This phenomenon is expected to affect the Stage IV and *CloudSat* retrievals equally and should therefore not significantly alter relative detections made by the two products.

3. Results

a. Regional detection characteristics

The collocation of Stage IV with *CloudSat* allows for comparisons at the individual pixel level, as opposed to comparing distributions of aggregated samples. To be included in the analysis, both *CloudSat* and Stage IV must each produce a valid retrieval for a collocated pair of observations. This encourages the use of a 2 × 2 contingency table to summarize the four possible combinations of the binary datasets. In Table 1, the variable *a* refers to the number of times that both Stage IV and *CloudSat* report precipitation in a collocated pair of observations. Variables *b* and *c* represent the number of times Stage IV reports precipitation but *CloudSat* does not and the number of times *CloudSat* reports precipitation but Stage IV does not, respectively. Variable *d* represents the number of times neither Stage IV nor *CloudSat* report precipitation. Throughout the remainder of this study, contingency table variables *a*, *b*, and *c* are referred to as Both, Stage IV Only, and *CloudSat* Only, respectively, to clarify their underlying meanings.

TABLE 1. A 2 × 2 contingency table where Stage IV does or does not observe precipitation and where *CloudSat* does or does not observe precipitation. Here *a*, *b*, and *c* are equal to relative precipitation detections as Both, Stage IV Only, and *CloudSat* Only, respectively. The value of *d* (no precipitation detected by either retrieval) typically takes a value much greater than the others because of the rarity of precipitation in our atmosphere.

	CloudSat yes	*CloudSat* no
Stage IV yes	*a*	*b*
Stage IV no	*c*	*d*

Figure 3a shows the overall percentages of FOVs found to be precipitating by the Stage IV and *CloudSat* for each basin for all collocated observations in 2007–10. *CloudSat* reports higher values of occurrence in all basins. Since this study is focused on differences between the two products, Fig. 3b shows relative precipitating detections for matched observations, where Stage IV Only, *CloudSat* Only, and Both as defined above. For example, the total precipitation percentage sensed by the *CloudSat* in the Ohio (OH) basin is represented by the sum of the Both and *CloudSat* Only values in this basin, which is shown in Fig. 3a as about 12%. *CloudSat* clearly reports precipitation more frequently than Stage IV across all RFC basins, with retrievals being similar only in the Arkansas–Red Basin (AB), West Gulf (WG), Lower Mississippi (LM), and Southeast (SE) regions. These basins reside in the south central and southeastern United States, where precipitation generally falls as rain and rarely as snow or sleet. On the other hand, large discrepancies can be seen in the California–Nevada (CN), Northwest (NW), and other basins. As will be shown, this is most likely due to the presence of light or frozen precipitation, which occurs frequently in the northern states. Differences in detection based exclusively on unavoidable collocation offsets (e.g., Fig. 2) are most directly represented in the Stage IV Only values in Fig. 3b. Since *CloudSat* is so sensitive to precipitation, the nonzero values of Stage IV Only are likely a result of a combination of advection offsets near edges of precipitation systems or where *CloudSat* makes its near-instantaneous measurement before or after the precipitation occurs (e.g., Fig. 2, orbit A) within the Stage IV hourly accumulation period. The influence of these effects is a strong function of the true precipitation fraction, its type, and the degree of organization of individual precipitation events in each basin. Differences between the total *CloudSat* and Stage IV precipitation

fractions in Fig. 3a include contributions from these collocation offsets as well as differences in precipitation detection ability. Since the spatial collocation offsets are small and random (not shown) and temporal sampling effects favor increasing Stage IV Only, these differences represent a conservative estimate of the fraction of precipitation occurrences that goes undetected in each RFC basin.

It is important to note that the requirement of collocated samples restricts the analysis to when *CloudSat* is ascending or descending over the CONUS, at approximately 0130 and 1330 LT due to its sun-synchronous polar orbit. Thus, the statistics presented here represent only a subset of the events contributing to precipitation patterns across the CONUS, allowing the study to highlight differences in the precipitation detection capabilities of Stage IV and *CloudSat*. The study cannot, for example, quantify the effects of the diurnal cycle on total precipitation probability in any given area. Despite this restriction, Fig. 3a illustrates that some basins exhibit well-understood patterns of precipitation, despite the restriction of time of the *CloudSat* time of overpass. This includes high precipitation frequency detected by *CloudSat* in the NW and Northeast (NE) basins and low precipitation frequency in the WG and AB basins, to name a few. Furthermore, it will be shown below that these comparisons provide valuable insights into the causes of precipitation detection biases that can be attributed to well-understood characteristics of ground-based S-band radars.

The frequencies of precipitation detected by *CloudSat* and Stage IV for all 48 months at 3° × 3° resolution are presented in Fig. 4 (left). With the exception of the southern states, values of Stage IV Only precipitation are very small here, ranging from 1.5% to 2%, while values of *CloudSat* Only and Both vary with precipitation type, organization, and frequency. Low values of Stage IV Only and Both are apparent in the northwest despite high values of *CloudSat* Only in the same area, owing to the frequent shallow, light precipitation falling in northern California and Oregon. The highest values of Both tend to occur in the northeastern CONUS, where precipitation tends to be more persistent in the winter than in the summer (Kursinski and Mullen 2008). If other factors are identical, a more organized precipitation system such as slow moving or frontal precipitation will produce better agreement between Stage IV and *CloudSat* than scattered, fast-moving, or small-scale precipitation because there are fewer spatial and temporal offsets in collocation. That, coupled with relatively good radar coverage (Maddox et al. 2002), could create a better environment for Stage IV to detect precipitation.

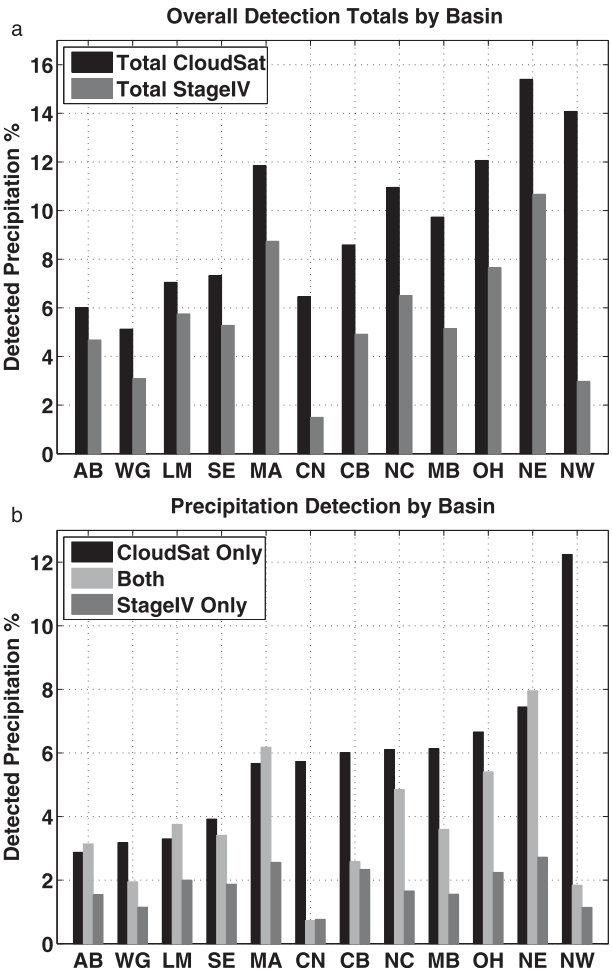

FIG. 3. (a) The overall percentage of collocated FOVs found to be precipitating as reported by Stage IV and *CloudSat* during 2007–10. (b) Percentages of relative detections for where Stage IV observes precipitation but *CloudSat* does not (Stage IV Only), for where *CloudSat* observes precipitation but Stage IV does not (*CloudSat* Only), and for where both Stage IV and *CloudSat* observe precipitation (Both) for collocated FOVs in each RFC basin over the CONUS. The x axes in each panel have been sorted to show increasing *CloudSat* Only for viewing purposes.

Significant amounts of *CloudSat* Only precipitation are also evident in the Great Lakes and Intermountain West regions in Fig. 4, providing a hint that snowfall may also play a role in detection differences between the two sensors. To examine this more closely, the middle and right columns of Fig. 4 show the comparisons for which the 2-m air temperature $T > 10°C$ and $T < 0°C$, respectively, as determined by the collocated ECMWF-AUX product (Partain 2007). Grid boxes containing greater than 25% *CloudSat* standard error (STE) are omitted. Standard errors are computed using Eq. (1), where N_p and N_t are the effective degrees of freedom for precipitating and total FOVs, respectively:

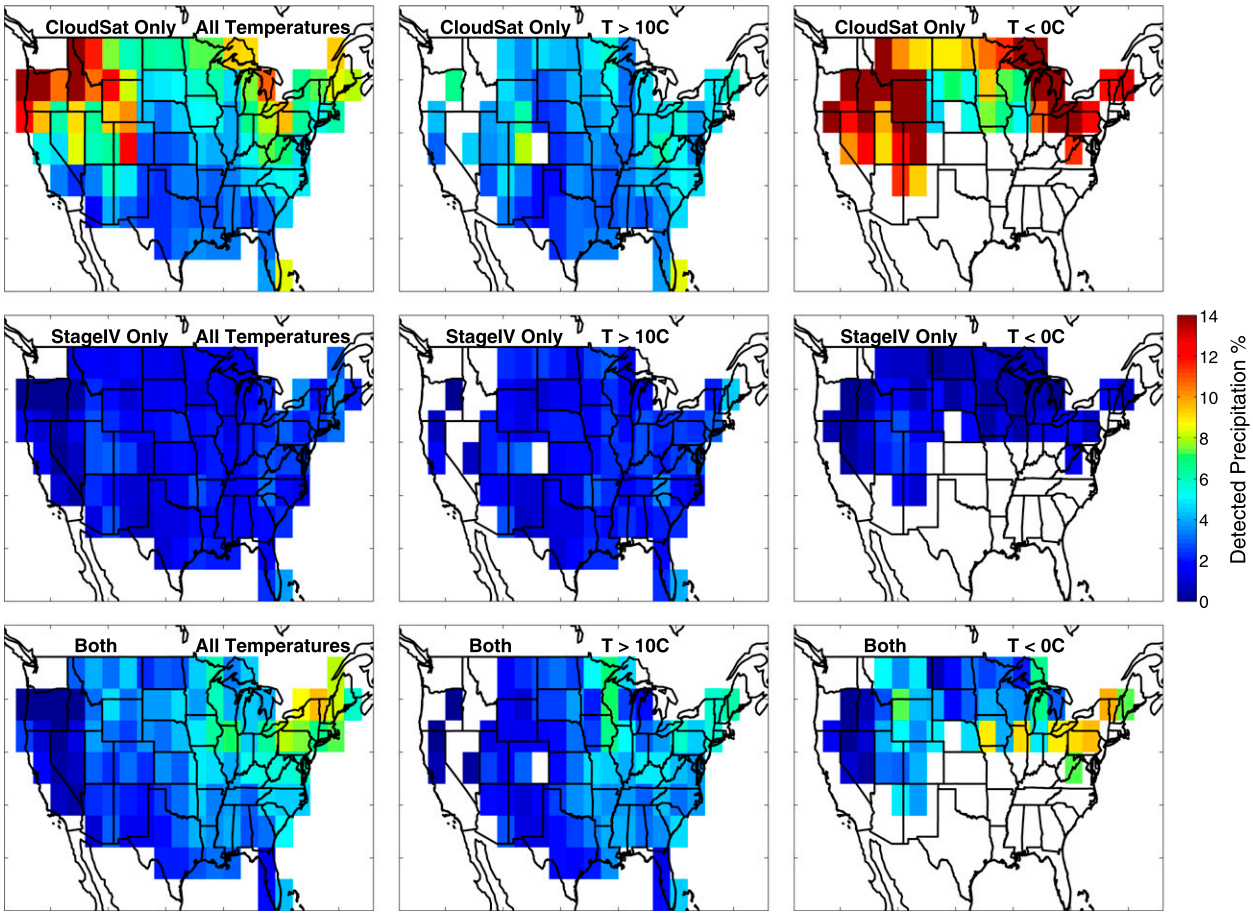

FIG. 4. Relative statistics for 48 months of collocated Stage IV and *CloudSat* precipitation detections. (left) Data from all temperatures;, (middle),(right) only data for which the 2-m near-surface air temperatures from ECMWF are >0°C and <0°C, respectively. Grid boxes are omitted if the corresponding *CloudSat* standard errors are found to be >25%, as computed by Eq. (1).

$$\mathrm{STE} = 100\sqrt{1/N_p + 1/N_t}. \qquad (1)$$

Effective degrees of freedom N_p and N_t are calculated using the method of Eq. (3) in L'Ecuyer et al. (2009). Areas with high standard error are indicative of regions with insufficient numbers of samples and/or precipitating retrievals in the corresponding temperature range and are omitted from display. This is particularly evident in the far west for warm conditions and in the south for cold conditions.

Retrievals from the *CloudSat* are used for determining the standard error for data filtering because the *CloudSat* precipitation detection is more sensitive to hydrometeors than the Stage IV precipitation detection. Detection differences are far greater when $T < 0°C$, where *CloudSat* observes much more precipitation than Stage IV across all presented areas. This supports the idea that the greater sensitivity of the CPR allows *CloudSat* to more readily detect frozen precipitation than Stage IV and may have important implications for applications seeking to constrain snowfall frequency or accumulations, including those seeking to model changes in snowpack or spring runoff. Stage IV and *CloudSat* exhibit better agreement for warm environment retrievals in Fig. 4 (middle), owing to the exclusive presence of liquid precipitation, which is more easily observed by the Stage IV. *CloudSat* still observes a greater amount of precipitation, likely because of reduced sensitivity and increased beam height at ranges far from radars in the Stage IV dataset, but discrepancies are much larger during the colder seasons.

b. Temperature dependence

To further assess the effect of near-surface air temperature, observations were sorted into 5°C bins based on collocated ECMWF 2-m air temperature for the entire CONUS. Figure 5 shows the resulting histogram of detection differences during all 48 months, along with the associated standard errors. Since the two retrievals have been collocated and therefore have exactly the

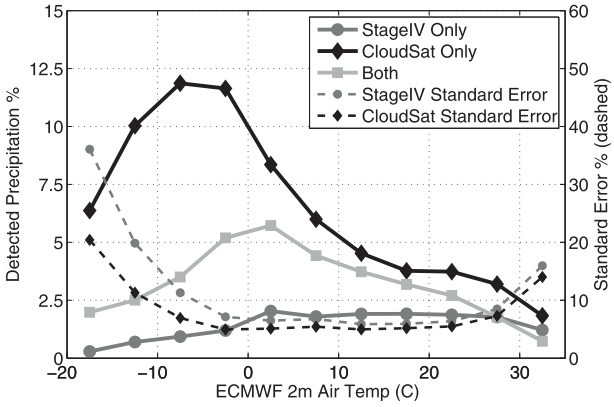

FIG. 5. Temperature dependence of relative precipitation detections between Stage IV and *CloudSat*. Standard errors are included as dashed lines using the *y* axis at the right. The large increase in *CloudSat* Only at and below 0°C is indicative of frozen precipitation likely unobserved by Stage IV but observed by *CloudSat* because of its high sensitivity to low reflectivities. Again, data are omitted where the *CloudSat* standard error is >25%.

same number of samples, differences in standard errors between *CloudSat* and Stage IV at a particular temperature range are a direct result of the differences in the number of precipitating scenes reported by each product. *CloudSat* observes more precipitation than Stage IV in all temperature ranges, so estimates of its standard errors are consequently lower. It is clear from Fig. 5 that values of *CloudSat* Only increase dramatically while values of Stage IV Only decrease when near-surface air temperatures are around −10° to 0°C. Hobbs et al. (1974) show that the ice aggregation process experiences a maximum when temperatures are between −10° and 0°C (Hobbs et al. 1974), which is consistent with the location of the *CloudSat* maximum in Fig. 5. From the addition of the *CloudSat* Only and Both data, Fig. 5 is also consistent with the fact that precipitation over the CONUS is less frequent at extreme temperatures. Kursinski and Mullen (2008) find that precipitation tends to be most common when temperatures are close to freezing because of the increased organization and lifetime of winter precipitation. The decrease in retrieved precipitation percentages in each Stage IV and *CloudSat* at very cold temperatures parallels a decreased affinity for existence of snow aggregates (Hobbs et al. 1974), which have larger cross sections that are more likely to be sensed by radar. The resulting lack of precipitation at extreme temperatures raises the standard error beyond the threshold chosen for this study.

Figure 6 illustrates the temperature-dependent detection characteristics of Stage IV and *CloudSat* in each

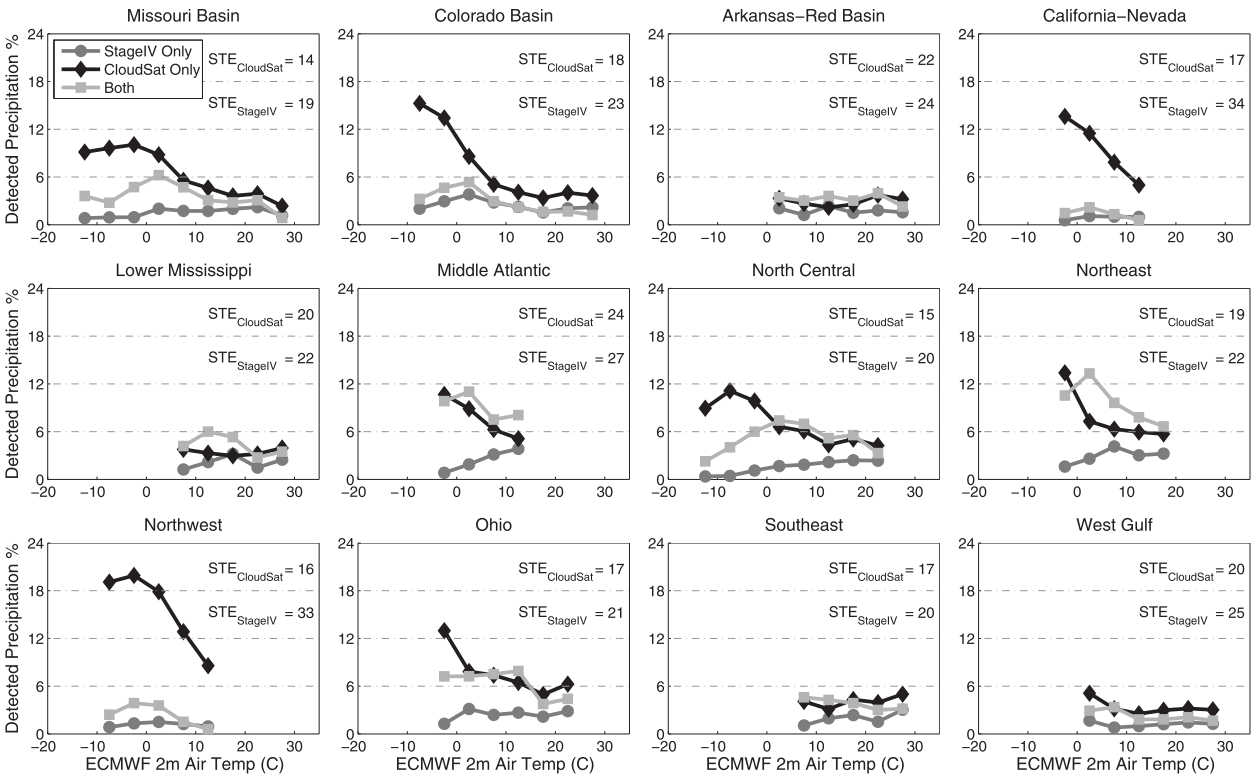

FIG. 6. As in Fig. 5, but separated for each RFC basin. Results are omitted if the corresponding *CloudSat* standard error is >25%. $STE_{CloudSat}$ and $STE_{Stage\,IV}$ represent the mean of the *CloudSat* and Stage IV standard errors for displayed data in each basin.

individual RFC basin. The results are generally consistent with knowledge of the meteorology of the respective regions. For example, the Missouri (MB), Colorado (CB), North Central (NC), and NE basins receive relatively large amounts of annual snowfall, and their respective subplots all indicate large discrepancies between the *CloudSat* and Stage IV precipitation fractions when near-surface air temperatures are close to or below freezing. Conversely, precipitation detections are in much closer agreement in southeastern basins, namely, the AB, LM, SE, and WG basins, which are characterized by convective precipitation with high rain rates that are easily observed by both *CloudSat* and Stage IV (Lin and Hou 2012). The NW and CN basins exhibit large differences in detection across all 2-m air temperature ranges. This is likely due to a combination of sparse radar coverage (Maddox et al. 2002), the prevalence of light but persistent stratiform precipitation along the west coast of the United States in the NW and CN basins, and frequent snowfall in the mountains and inland portions of the NW basin. In contrast to *CloudSat* Only, the values of Stage IV Only decrease with decreasing temperatures below 0°C from already lesser values in all basins for which data are displayed.

c. *Quantifying detection differences*

To further quantify differences in the precipitation detection characteristics of *CloudSat* and Stage IV, skill scores are computed for each region and temperature range. Because of the high sensitivity of the CPR to all types of precipitation, it is reasonable to use *CloudSat* as a reference observation and consider the Stage IV as the "model" or "forecast" of precipitation, although it should be emphasized that the *CloudSat* dataset does not represent an absolute truth. This allows the bias, Peirce skill score (PSS), and odds ratio skill score (ORSS, also known as Yule's Q) to be used to estimate the proficiency of the Stage IV precipitation detection relative to *CloudSat* in a manner analogous to testing binary forecasts of precipitation occurrence using a forecast/observation contingency table shown in Table 1. Equation (2) summarizes the definitions of the different scores and how they relate to the contingency variables a, b, c, and d in Table 1:

$$\begin{aligned} \text{bias} &= \frac{a+b}{a+c} \\ \text{PSS} &= \frac{ab-bc}{(a+c)(b+d)} = H - F \\ \text{ORSS} &= \frac{(ad/bc)-1}{(ad/bc)+1} = \frac{ad-bc}{ad+bc}. \end{aligned} \tag{2}$$

The bias (Wilks 2011) is the ratio of predicted positive outcomes to observed positive outcomes of a binary forecast. It can take values from 0 (no predicted positive outcomes) to 1 (even number of predicted positive outcomes and observed positive outcomes) to infinity (no positive observed outcomes). The bias is used to assess whether Stage IV or *CloudSat* reports more occurrences of precipitation. The PSS (Peirce 1884) takes the value of 1 for perfect forecasts (hit rate $H = 1$ and false alarm rate $F = 0$), 0 for unbiased random forecasts ($H = F$) and constant forecasts, and -1 for perfectly incorrect forecasts. The PSS has the advantage of giving greater weight to correct forecasts of rare events, which is the case with precipitation. Similarly, the ORSS (Yule 1900) takes values of 1 for perfect forecasts, 0 for random forecasts, and -1 for perfectly incorrect forecasts. A drawback of using the ORSS is that it results in a perfect forecast if either b or c is 0, which could simply be a result of low sample sizes. However, this weakness is mitigated by the inclusion of an estimate of uncertainty, which indicates if a low number of samples in any one value in Table 1 might adversely affect the robustness of the ORSS estimate. As shown by Stephenson (2000), the PSS, ORSS, and bias can be used to fully describe the three degrees of freedom in a 2×2 contingency table, as long as uncertainties are respected for the PSS and ORSS. Confidence intervals of 95% are computed using Eq. (3), where uncertainty estimates for the PSS and ORSS are taken from Wilks (2011, his Eq. 8.83) and Bishop et al. (1975, their Eq. 11.2–11), respectively:

$$\begin{aligned} \text{CI}_{\text{PSS}} &= \pm 1.96\sqrt{\frac{N_r^2 - 4(a_r+c_r)(b_r+d_r)\text{PSS}^2}{4N_r(a_r+c_r)(b_r+d_r)}} \\ \text{CI}_{\text{ORSS}} &= \pm 1.96(1-\text{ORSS}^2)\frac{1}{2}\sqrt{\frac{1}{a_r}+\frac{1}{b_r}+\frac{1}{c_r}+\frac{1}{d_r}}. \end{aligned} \tag{3}$$

In Eq. (3), the subscript r indicates that the value has been multiplied by the ratio of the reduced degrees of freedom to the number of observations pairs (N_r/N) used to calculate each value of PSS and ORSS. This is done to account for high autocorrelation found in both datasets, which violates the assumption of independent draws of observations that fill the contingency table.

Figure 7 shows changes in the PSS, ORSS, and bias with collocated ECMWF 2-m air temperature in each RFC. Several general distinctive characteristics are immediately visible in Fig. 7. First, the bias is rarely near 1 and almost never greater than 1, confirming that *CloudSat* detects more frequent precipitation than Stage IV at all temperature ranges in all basins except in the AB between 10° and 15°C and the LM between 15° and 20°C, where the bias is just above 1. The analogous plots in Fig. 6 show that values of Stage IV Only and *CloudSat*

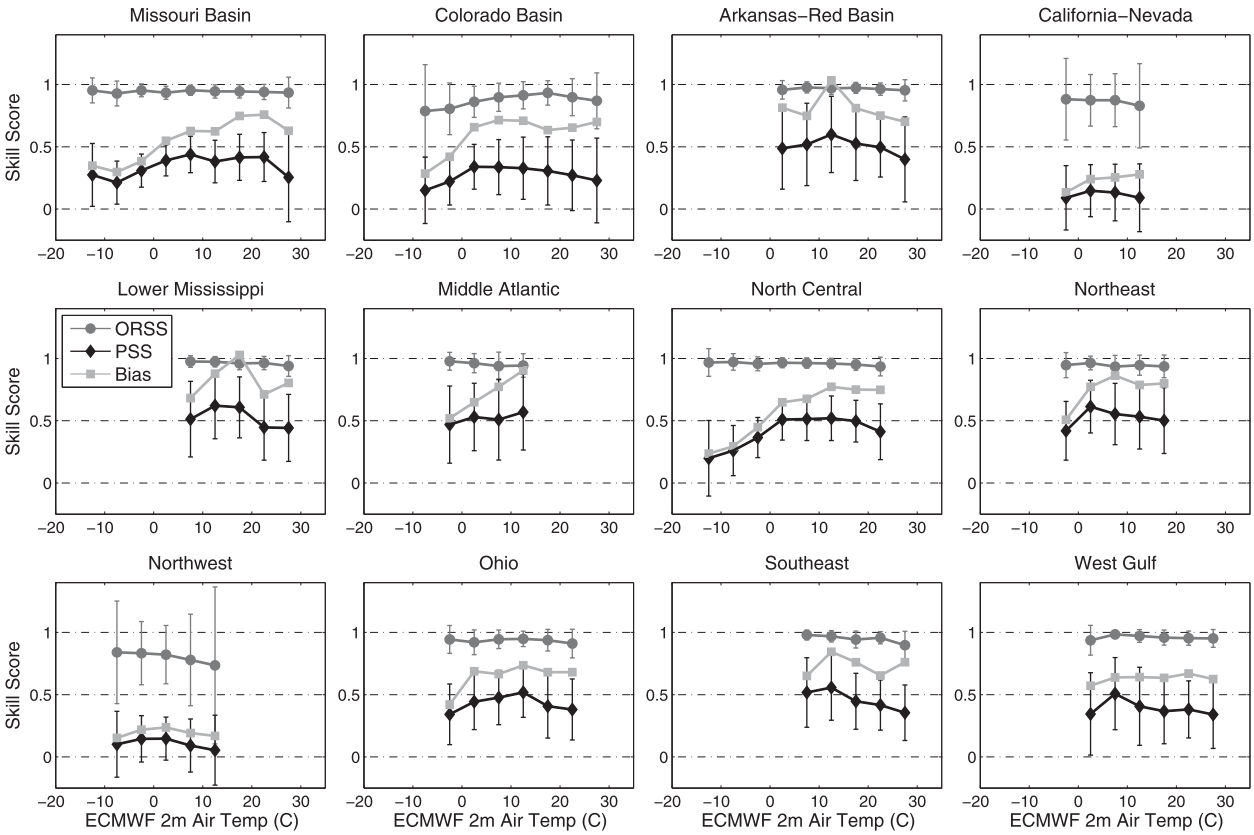

FIG. 7. Estimates of the ORSS, PSS, and bias for comparisons of detection statistics, as computed from Eq. (2) for the various basins. The 95% confidence intervals are estimated from Eq. (2). Scores are omitted from the figure if the corresponding *CloudSat* standard error is >25%.

Only are each around 2.5% at these temperatures while the value of Both is about twice as high, indicating great agreement between *CloudSat* and Stage IV in these conditions. Precipitation at these temperatures and locations is certainly rain, which is ideal for the WSR-88D radar retrievals. Basins having near-surface air temperatures below zero consistently exhibit low PSS and bias, consistent with the decreased ability of Stage IV to measure snow and mixed precipitation. This further emphasizes the difficulty that the WSR-88D radars have in detecting frozen precipitation but helps to place this effect in more quantitative terms. According to the uncertainty analysis, this study is not able to say with 95% confidence that Stage IV has nonzero skill in the NW at any temperature. This is another indication of the complex terrain in the area and lack of radar sites and sensitivity that are necessary to retrieve the light rain and frozen precipitation that characterizes the NW.

It is interesting to note that the ORSS does not appear to exhibit the decreasing trend at cold temperatures, while the PSS does. Equation (2) shows that the ORSS puts an equal emphasis on correct positive forecasts (precipitation) and correct negative forecasts (no precipitation). In this case, the values of the ORSS are skewed toward unity by the nature of precipitation being a relatively rare event in comparison to lack of precipitation. The ORSS is therefore dominated by nonprecipitating scenes and demonstrates that the sensors tend to agree that these occur far more frequently than precipitation in all regions and temperature ranges. This illustrates the importance of reporting more than one skill score, as simple presentation of the ORSS alone would convey an unrealistically high skill of Stage IV in detecting precipitation. In contrast, the PSS places greater emphasis on the correct positive forecasts and marginal totals of the contingency table and consequently takes lower values in all basins in Fig. 7.

4. Discussion

Many applications of the Stage IV data focus on the amount of accumulated precipitation, rather than the frequency of precipitation. Because the fourth release of the 2C-PRECIP-COLUMN dataset used here does not

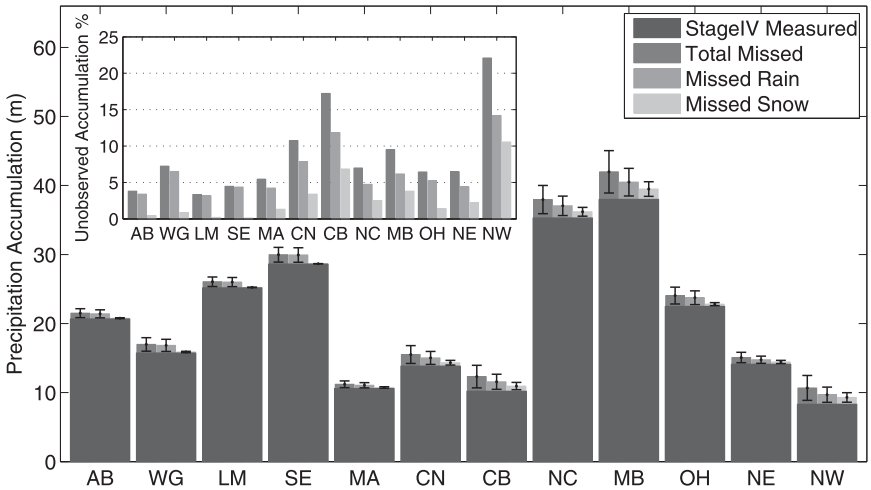

FIG. 8. Stage IV measured accumulations (water equivalent) for collocated FOVs by basin with estimates of unobserved accumulations of rain, mixed plus snow (labeled snow), and the total of the two. The inset figure shows the estimated amount of unobserved accumulations by Stage IV in each basin as a percentage of the total plus unobserved accumulations.

include estimates of precipitation rates, it is not currently possible to use the *CloudSat* to rigorously quantify the accumulation that may result from precipitation that is not detected by Stage IV. However, it is possible to provide a ballpark estimate based on an approximate estimate of the sensitivity of the WSR-88D rain rate retrievals. Unmeasured accumulations can then be estimated from using the number of missed collocated precipitating FOVs by applying standard Z–R and Z–S relationships (Battan 1973, his Tables 7-1 and 7-3). As before, only occurrences of rain certain, mixed certain, and snow certain are included in the calculation.

CloudSat identifies a pixel as containing precipitation if its near-surface reflectivity is greater than about 0 dBZ (section 2b). Conversely, a typical threshold assumed for discriminating rain in WSR-88D QPE algorithms is 15 dBZ (Hartzell et al. 2001). In the absence of total beam blockage or overshoot, then, these limits provide useful estimates for the range of reflectivities that the CPR would report as precipitating but the Stage IV would not. To assess the magnitude of unmeasured accumulations in each RFC, individual precipitation rates at 0 and 15 dBZ were computed using all Z–R and Z–S relationships found in Battan (1973, his Tables 7-1 and 7-3). The resulting liquid-equivalent precipitation rates were averaged and multiplied by the number of unobserved rainy and snowy FOVs as reported by the scaled *CloudSat* 2C-PRECIP-COLUMN dataset.

Figure 8 shows both observed Stage IV accumulations for collocated FOVs and the corresponding estimates of unobserved accumulation. Clearly Stage IV captures the majority of precipitation in all basins, but in some cases a significant fraction of the total accumulation may be missing from the Stage IV record, as shown in the inset. For example, about 17% and 22% of water volume may be absent from the CB and NW, respectively. This value would likely move to even higher percentages if data from the Washington State area were included in the hourly Stage IV product (Westrick et al. 1999). Consistent with precipitation occurrences, basins in the south and southeastern United States tend to miss less precipitation volume than their northern counterparts. Even so, this rough calculation suggests that ~5% of precipitation volume may be missed in any RFC. When coupled with biases in precipitation frequency, such estimates could have implications for modeling changes in soil moisture, estimating turbulent heat fluxes, and assessing regional climate variability. It may also be important to account for such effects when using Stage IV to evaluate other rainfall accumulation products such as those from Tropical Rainfall Measuring Mission (TRMM) and Global Precipitation Measurement (GPM; Lin and Hou 2012).

Again, it should be emphasized that the results in Fig. 8 provide only ballpark estimates of the precipitation missed by Stage IV and its relative contribution in each RFC. True accumulations in any given basin are not possible without quantitative intensity retrievals for each *CloudSat* FOV and will even then be limited by the sun-synchronous orbit of *CloudSat*. It is worth noting that the next release of the *CloudSat* rain rate algorithm will provide rate estimates of rain and snow over land regions that should provide a more direct measure of the volume of precipitation missing from the Stage IV and other records.

5. Conclusions

This study shows that, because of a combination of limited radar density, beam blockage and overshoot, and limited sensitivity to frozen precipitation, the Stage IV hourly precipitation accumulation product may underrepresent precipitation occurrences across the contiguous United States, including as much as 78% of precipitation occurrences in the Northwest basin. While the undetected precipitation events may often be composed of light or frozen precipitation that do not generally result in flooding events, these precipitation types, especially snowfall, can be frequent enough to contribute significantly to local water budgets, affect soil moisture, and influence the strength of local turbulent heat and moisture fluxes. Undetected snowfall also affects snowmelt runoff in the spring season, which is important for water resources and flood mitigation. The following conclusions can be drawn from this analysis.

1) Regions with dense radar coverage and typically heavy or large-scale precipitation events exhibit the best agreement between Stage IV and *CloudSat.* This generally includes areas from the south-central to eastern portions of the United States.
2) A maximum of missed precipitation occurs in the northwestern United States, corresponding to climatologically light rain along the coast, snowfall inland, and sparse regional radar coverage and beam blockage.
3) A secondary maximum of missed precipitation occurs in the northeastern United States, corresponding to regional cold season snowfall.
4) The majority of undetected precipitation events occur when near-surface air temperatures fall below 0°C. This trait is common to all RFC basins having substantial cold season precipitation.
5) Skill score analysis shows that Stage IV systematically observes fewer precipitation events than *CloudSat*, and the performance of Stage IV when compared to *CloudSat* decreases when near-surface air temperatures drop below 0°C.

Acknowledgments. This work was supported by NASA *CloudSat*/*CALIPSO* Science Team (CCST) Grant NNX12AC51G. The authors acknowledge the efforts made at the *CloudSat* Data Processing Center (http://www.cloudsat.cira.colostate.edu) and the National Center for Atmospheric Research (NCAR) Earth Observing Laboratory (EOL) (http://www.emc.ncep.noaa.gov/mmb/ylin/pcpanl/stage4/) in making these data available.

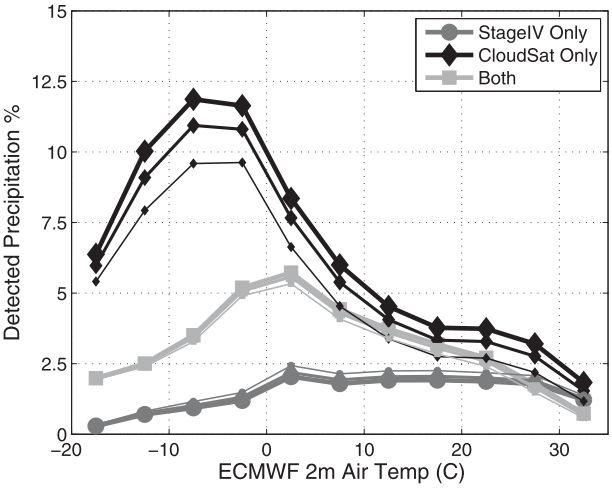

FIG. A1. Effect of scaling the *CloudSat* precipitation flag as a function of temperature. The thin, medium, and thick lines represent results when using the nominal *CloudSat* resolution, three *CloudSat* FOVs, and five *CloudSat* FOVs (used in this study) to scale the *CloudSat* precipitation detections to approximate the resolution of the Stage IV QPEs. Scaling the *CloudSat* data does not affect the general trends in detection differences.

APPENDIX

Effects of Spatial Resolution

As noted in section 2c, precipitation occurrences from *CloudSat* at ~1.5-km resolution were scaled up to more closely match the ~4.7-km spatial resolution of Stage IV. Because of the binary nature of the *CloudSat* 2C-PRECIP-COLUMN product, this can only serve to increase the rate of detections by *CloudSat*. To demonstrate that these effects are not responsible for the differences in detection characteristics between *CloudSat* and Stage IV, the effects of spatial scaling on the results are illustrated in Fig. A1. Precipitation occurrence over the entire CONUS is determined from matched observations at the nominal *CloudSat* resolution, an average of three *CloudSat* FOVs, and the average of five *CloudSat* FOVs chosen in this study as providing the best match to the Stage IV grid. Recall that in each case an averaged FOV is found to be precipitating if any of the constituent FOVs is found to be precipitating. As expected, scaling the *CloudSat* data clearly increases fractions of *CloudSat* Only, but it also slightly decreases values of Stage IV Only while increasing values of Both by a small amount at all temperatures. In this way, scaled *CloudSat* retrievals gain precipitation detections that the nominal resolution retrievals miss when the *CloudSat* measurements may have taken place just before of after precipitation occurrence in the Stage IV grid box. This is likely at the

edge of a precipitating system and effectively shifts Stage IV Only precipitation into the Both category. On the other hand, increases in *CloudSat* Only are likely due to precipitation occurrences that are missed by Stage IV, causing it to increase somewhat proportionally in all temperature ranges. It is seen that, although the scaling does increase the value of *CloudSat* Only in relation to Stage IV Only and Both, the effect is small compared to the overall magnitude of precipitation occurrences missed by Stage IV and does not affect the systematic pattern with temperature in the results. Therefore, even though this scaling is appropriate since the Stage IV dataset is generated from polar 1° km × 1 km rain rates within the NWS PPS, it is encouraging to see that the results are not strongly influenced by this averaging.

REFERENCES

Battan, L. J., 1973: *Radar Observation of the Atmosphere.* University of Chicago Press, 324 pp.

Behrangi, A., M. Lebsock, S. Wong, and B. Lambrigtsen, 2012: On the quantification of oceanic rainfall using spaceborne sensors. *J. Geophys. Res.,* **117,** D20105, doi:10.1029/2012JD017979.

Berg, W., T. L'Ecuyer, and J. M. Haynes, 2010: The distribution of rainfall over oceans from spaceborne radars. *J. Appl. Meteor. Climatol.,* **49,** 535–543, doi:10.1175/2009JAMC2330.1.

Bishop, Y. M., S. E. Fienberg, and P. W. Holland, 1975: *Discrete Multivariate Analysis: Theory and Practice.* MIT Press, 557 pp.

Cao, Q., Y. Hong, J. J. Gourley, Y. Qi, J. Zhang, Y. Wen, and P.-E. Kirstetter, 2013: Statistical and physical analysis of the vertical structure of precipitation in the mountainous west region of the United States using 11+ years of spaceborne observations from TRMM precipitation radar. *J. Appl. Meteor. Climatol.,* **52,** 408–424, doi:10.1175/JAMC-D-12-095.1.

Ellis, T. D., T. L'Ecuyer, J. M. Haynes, and G. L. Stephens, 2009: How often does it rain over the global oceans? The perspective from CloudSat. *Geophys. Res. Lett.,* **36,** L03815, doi:10.1029/2008GL036728.

Fulton, R., cited 2005: Multisensor Precipitation Estimator (MPE) Workshop. [Available online at http://www.nws.noaa.gov/oh/hrl/papers/wsr88d/MPE_workshop_NWSTC_lecture2_121305.pdf.]

——, J. P. Breidenbach, D.-J. Seo, and D. A. Miller, 1998: The WSR-88D rainfall algorithm. *Wea. Forecasting,* **13,** 377–395, doi:10.1175/1520-0434(1998)013<0377:TWRA>2.0.CO;2.

Gourley, J. J., Y. Hong, Z. L. Flamig, L. Li, and J. Wang, 2010: Intercomparison of rainfall estimates from radar, satellite, gauge, and combinations for a season of record rainfall. *J. Appl. Meteor. Climatol.,* **49,** 437–452, doi:10.1175/2009JAMC2302.1.

Habib, E., B. F. Larson, and J. Graschel, 2009: Validation of NEXRAD multisensor precipitation estimates using an experimental dense rain gauge network in south Louisiana. *J. Hydrol.,* **373,** 463–478, doi:10.1016/j.jhydrol.2009.05.010.

——, L. Qin, D. Seo, G. J. Ciach, and B. R. Nelson, 2013: Independent assessment of incremental complexity in NWS multisensor precipitation estimator algorithms. *J. Hydrol. Eng.,* **18,** 143–155, doi:10.1061/(ASCE)HE.1943-5584.0000638.

Hartzell, C. L., S. M. Hunster, and E. W. I. Holroyd, 2001: Development of a WSR-88D based precipitation accumulation algorithm for quantitative precipitation estimates over northwest Oregon. Preprints, *17th Int. Conf. on Interactive Information and Processing Systems for Meteorology, Oceanography, and Hydrology,* Albuquerque, NM, Amer. Meteor. Soc., 146–150.

Haynes, J. M., T. S. L'Ecuyer, G. L. Stephens, S. D. Miller, C. Mitrescu, N. B. Wood, and S. Tanelli, 2009: Rainfall retrieval over the ocean with spaceborne W-band radar. *J. Geophys. Res.,* **114,** D00A22, doi:10.1029/2008JD009973.

Hobbs, P. V., S. Chang, and J. D. Locatelli, 1974: The dimensions and aggregation of ice crystals in natural clouds. *J. Geophys. Res.,* **79,** 2199–2206, doi:10.1029/JC079i015p02199.

Hudak, D., P. Rodriguez, and N. Donaldson, 2008: Validation of the CloudSat precipitation occurrence algorithm using the Canadian C band radar network. *J. Geophys. Res.,* **113,** D00A07, doi:10.1029/2008JD009992.

Kursinski, A. L., and S. L. Mullen, 2008: Spatiotemporal variability of hourly precipitation over the eastern contiguous United States from stage IV multisensor analyses. *J. Hydrometeor.,* **9,** 3–21, doi:10.1175/2007JHM856.1.

Lebsock, M. D., and T. S. L'Ecuyer, 2011: The retrieval of warm rain from CloudSat. *J. Geophys. Res.,* **116,** D20209, doi:10.1029/2011JD016076.

L'Ecuyer, T., and G. Stephens, 2002: An estimation-based precipitation retrieval algorithm for attenuating radars. *J. Appl. Meteor.,* **41,** 272–285, doi:10.1175/1520-0450(2002)041<0272:AEBPRA>2.0.CO;2.

L'Ecuyer, T. S., W. Berg, J. Haynes, M. Lebsock, and T. Takemura, 2009: Global observations of aerosol impacts on precipitation occurrence in warm maritime clouds. *J. Geophys. Res.,* **114,** D09211, doi:10.1029/2008JD011273.

Lin, X., and A. Y. Hou, 2012: Estimation of rain intensity spectra over the continental United States using ground radar–gauge measurements. *J. Climate,* **25,** 1901–1915, doi:10.1175/JCLI-D-11-00151.1.

Lin, Y., and K. E. Mitchell, 2005: The NCEP stage II/IV hourly precipitation analyses: Development and applications. Preprints, *19th Conf. on Hydrology,* San Diego, CA, Amer. Meteor. Soc., 1.2. [Available online at https://ams.confex.com/ams/pdfpapers/83847.pdf.]

Maddox, R., J. Zhang, J. Gourley, and K. Howard, 2002: Weather radar coverage over the contiguous United States. *Wea. Forecasting,* **17,** 927–934, doi:10.1175/1520-0434(2002)017<0927:WRCOTC>2.0.CO;2.

Marchand, R., G. G. Mace, T. Ackerman, and G. Stephens, 2008: Hydrometeor detection using *CloudSat*—An Earth-orbiting 94-GHz cloud radar. *J. Atmos. Oceanic Technol.,* **25,** 519–533, doi:10.1175/2007JTECHA1006.1.

Matrosov, S. Y., and A. Battaglia, 2009: Influence of multiple scattering on CloudSat measurements in snow: A model study. *Geophys. Res. Lett.,* **36,** L12806, doi:10.1029/2009GL038704.

Michaelides, S., V. Levizzani, E. Anagnostou, P. Bauer, T. Kasparis, and J. E. Lane, 2009: Precipitation: Measurement, remote sensing, climatology and modeling. *Atmos. Res.,* **94,** 512–533, doi:10.1016/j.atmosres.2009.08.017.

Nicosia, D. J., and Coauthors, 1999: A flash flood from a lake-enhanced rainband. *Wea. Forecasting,* **14,** 271–288, doi:10.1175/1520-0434(1999)014<0271:AFFFAL>2.0.CO;2.

Partain, P., 2007: CloudSat ECMWF-AUX auxiliary data process description and interface control document (algorithm

version 5.2). CloudSat Project Doc., 11 pp. [Available online at http://www.cloudsat.cira.colostate.edu/ICD/ECMWF-AUX/ECMWF-AUX_PDICD_5.2.doc.]

Peirce, C., 1884: The numerical measure of the success of predictions. *Science,* **ns-4,** 453–454, doi:10.1126/science.ns-4.93.453-a.

Stephens, G. L., and Coauthors, 2008: CloudSat mission: Performance and early science after the first year of operation. *J. Geophys. Res.,* **113,** D00A18, doi:10.1029/2008JD009982.

——, and Coauthors, 2010: Dreary state of precipitation in global models. *J. Geophys. Res.,* **115,** D24211, doi:10.1029/2010JD014532.

Stephenson, D. B., 2000: Use of the ''odds ratio'' for diagnosing forecast skill. *Wea. Forecasting,* **15,** 221–232, doi:10.1175/1520-0434(2000)015<0221:UOTORF>2.0.CO;2.

Tanelli, S., S. L. Durden, K. S. Pak, D. G. Reinke, P. Partain, J. M. Haynes, and R. T. Marchand, 2008: CloudSat's cloud profiling radar after two years in orbit: Performance, calibration, and processing. *IEEE Trans. Geosci. Remote Sens.,* **46,** 3560–3573, doi:10.1109/TGRS.2008.2002030.

Tao, K., and A. P. Barros, 2010: Using fractal downscaling of satellite precipitation products for hydrometeorological applications. *J. Atmos. Oceanic Technol.,* **27,** 409–427, doi:10.1175/2009JTECHA1219.1.

Tesfagiorgis, K., S. E. Mahani, N. Y. Krakauer, and R. Khanbilvardi, 2011: Bias correction of satellite rainfall estimates using a radar-gauge product—A case study in Oklahoma (USA). *Hydrol. Earth Syst. Sci.,* **15,** 2631–2647, doi:10.5194/hess-15-2631-2011.

Westcott, N. E., H. V. Knapp, and S. D. Hilberg, 2008: Comparison of gage and multi-sensor precipitation estimates over a range of spatial and temporal scales in the Midwestern United States. *J. Hydrol.,* **351,** 1–12, doi:10.1016/j.jhydrol.2007.10.057.

Westrick, K. J., C. F. Mass, and B. A. Colle, 1999: The limitations of the WSR-88D radar network for quantitative precipitation measurement over the coastal western United States. *Bull. Amer. Meteor. Soc.,* **80,** 2289–2298, doi:10.1175/1520-0477(1999)080<2289:TLOTWR>2.0.CO;2.

Wilks, D. S., 2011: *Statistical Methods in the Atmospheric Sciences*. 3rd ed. Academic Press, 704 pp.

Wu, W., D. Kitzmiller, and S. Wu, 2012: Evaluation of radar precipitation estimates from the National Mosaic and Multisensor Quantitative Precipitation Estimation System and the WSR-88D Precipitation Processing System over the conterminous United States. *J. Hydrometeor.,* **13,** 1080–1093, doi:10.1175/JHM-D-11-064.1.

Yuan, H., S. L. Mullen, X. Gao, S. Sorooshian, J. Du, and H.-M. H. Juang, 2005: Verification of probabilistic quantitative precipitation forecasts over the southwest United States during winter 2002/03 by the RSM ensemble system. *Mon. Wea. Rev.,* **133,** 279–294, doi:10.1175/MWR-2858.1.

——, X. Gao, S. L. Mullen, S. Sorooshian, J. Du, and H.-M. H. Juang, 2007: Calibration of probabilistic quantitative precipitation forecasts with an artificial neural network. *Wea. Forecasting,* **22,** 1287–1303, doi:10.1175/2007WAF2006114.1.

Yule, G. U., 1900: On the association of attributes in statistics. *Philos. Trans. Roy. Soc. London,* **A194,** 257–319, doi:10.1098/rsta.1900.0019.

Zhang, J., and Y. Qi, 2010: A real-time algorithm for the correction of brightband effects in radar-derived QPE. *J. Hydrometeor.,* **11,** 1157–1171, doi:10.1175/2010JHM1201.1.

——, C. Langston, and K. Howard, 2008: Brightband identification based on vertical profiles of reflectivity from the WSR-88D. *J. Atmos. Oceanic Technol.,* **25,** 1859–1872, doi:10.1175/2008JTECHA1039.1.